ELSEVIER

Remote Sensing of Environment 76 (2001) 354–366

Remote Sensing of Environment

www.elsevier.com/locate/rse

# A Spectralon BRF data base for MISR calibration applications

Carol Bruegge*, Nadine Chrien, David Haner

*Jet Propulsion Laboratory, California Institute of Technology, MS 169-237, 4800 Oak Grove Drive, Pasadena, CA 91109, USA*

**Abstract**

The Multi-angle Imaging SpectroRadiometer (MISR) is an Earth-observing sensor, which provides global retrievals of aerosols, clouds, and land surface parameters. Instrument specifications require an accurate absolute calibration, as well as accurate camera-to-camera, band-to-band and pixel-to-pixel relative response determinations. In order to achieve these requirements, MISR makes use of an on-board calibrator (OBC), as well as vicarious calibration (VC) experiments. The OBC makes use of two Spectralon diffuse panels in order to provide a flatfield illumination. Bi-monthly deployments of these panels into the camera fields-of-view will be made. At these times, solar-reflected radiance values are measured by photodiode detector standards. Accurate relative bidirectional reflectance factor (BRF) data are required to transfer these photodiode-measured radiances into camera-incident values. An independent calibration pathway, known as VC, will also be implemented in order to reduce systematic errors and to provide a crosscheck on the OBC findings. Here, the top-of-atmosphere radiances are computed from in situ observations of surface reflectance and atmospheric transmittances. Key to these measurements is knowledge of the hemispheric/directional reflectance factor (HDRF) of the field reflectance standards. This report describes the BRF measurements of the MISR flight panels, and provides an estimation as to the differences between HDRF and BRF for the MISR view angles. This BRF data base is available from the MISR web site, http://www-misr.jpl.nasa.gov. © 2001 Published by Elsevier Science Inc.

## 1. Introduction

Spectralon is a sintered polytetrafluoroethylene (PTFE) material manufactured by Labsphere. Spectralon panels are valued as reflectance standards in that they approach Lambertian behavior, particularly at near-nadir illumination angles, are nearly spectrally neutral across the visible and near-infrared (Labsphere, 1998), are machinable, weather-resistant, and washable. For these reasons, Spectralon is widely used in field validation experiments conducted in support of remote sensing systems. The material has been space-qualified (Bruegge, Duval, Chrien, & Diner, 1993) and has been built into the MISR on-board calibrator (OBC). Spectralon panels are also utilized on another of the Terra spacecraft instruments, the Moderate Resolution Imaging Spectroradiometer (MODIS).

For all applications in which MISR makes use of Spectralon views, knowledge of its bidirectional reflectance factor (BRF) is required. Few facilities have the capability to accurately measure BRF. For this reason, many have explored the suitability of a general calibration model for Spectralon (Jackson, Clarke, & Moran, 1992; Weidner & Hsia, 1981). Those that do have the capability of making BRF measurements typically quote principal plane measurements (Barnes et al., 1998; Early et al., 1999), or those for a nadir-viewing sensor. (The principal plane contains the source and view angle directions.) Only one other literature report describes the BRF at all viewing angles (Feng, Schott, & Gallagher, 1993). MISR, with its extreme range of viewing angles, requires such a complete mapping of BRF into the reflecting hemisphere.

### 1.1. Reflectance nomenclature

Following the nomenclature of Nicodemus, Richmond, Ginsberg, Hsia, and Limperis (1977), MISR will retrieve the bidirectional reflectance distribution factor (BRF), written as:

$$R(\theta_i, \phi_i; \theta_r, \phi_r) = d\Theta_r / d\Theta_{r,ideal}. \quad (1)$$

That is, for an irradiance incident at angle $\theta_i$,$\phi_i$, the reflected flux, $d\Theta_r$, in view angle direction $\theta_r$,$\phi_r$ is measured. This is ratioed to the flux from an ideal (i.e., lossless and perfectly diffuse) surface, $d\Theta_{r,ideal}$, irradiated in exactly the same way as the sample. Partial derivatives are used in the notation,

* Corresponding author.
*E-mail address*: carol.j.bruegge@jpl.nasa.gov (C. Hsia).


PII: S0034-4257(01)00214-0

signifying measurement over surface element d$A$. The BRF is an appropriate descriptor of the reflectance under point-source, narrow-cone beam illumination. It is thus suitable for direct use in MISR on-orbit calibration, where panel illumination occurs outside the Earth's atmosphere.

Throughout this paper, subscripts will be used to qualify properties of the angular and radiometric quantities. For illumination from a direct beam source, such as the Sun, we use the subscript o, for illumination at arbitrary angles, the subscript i, and all quantities associated with reflected flux are identified with the subscript r. The incident azimuth is defined as $\phi_i = 0°$; hence, reference to it is subsequently omitted. For the reflected beam, $\phi_r = 0°$ represents the backscattered azimuth direction and $\phi_r = 180°$ represents the forward scattered azimuth direction.

Expanding the numerator and denominator in Eq. (1) gives (Eq. (2)):

$$d\Theta_r = dA L_r(\theta_r, \phi_r)\cos\theta_r d\omega_r, \tag{2}$$

and

$$d\Theta_{r,ideal} = dA[E_i(\theta_i)/\pi]\cos\theta_r d\omega_r. \tag{3}$$

Eq. (3) comes about since the ideal diffuse surface reflects the same radiance, $E_i(\theta_i)/\pi$, in all view directions. Combining these produces:

$$R(\theta_i; \theta_r, \phi_r) = L_r(\theta_r, \phi_r)\pi / E_i(\theta_i). \tag{4}$$

For use in field applications, the incident irradiance consists of a mixture of solar (direct) and non-isotropic diffuse illumination. For this case, we utilize the hemispherical/directional reflectance factor (HDRF). This is still derived from Eqs. (1) and (4); however, now, the source of the incident irradiance includes a diffuse, non-isotropic component. We write (Eqs. (5), (6)):

$$d\Theta_r = \frac{dA\cos\theta_r}{\pi}\left[R(\theta_o; \theta_r, \phi_r)E_{dir}(\theta_o) + \int R(\theta_i, \phi_i; \theta_r, \phi_r)L_{dif}(\theta_i, \phi_i)d\omega_i\right] \tag{5}$$

$$d\Theta_{r,ideal} = \frac{dA\cos\theta_r}{\pi}\int L_{tot}(\theta_i, \phi_i)d\omega_i = \frac{dA\cos\theta_r E_{tot}}{\pi} \tag{6}$$

where (Eqs. (7)–(9))

$$d\omega_i = \sin\theta_i(d\theta_i)d\phi_i \tag{7}$$

$$E_{dif} = \int L_{dif}(\theta_i, \phi_i)d\omega_i, \tag{8}$$

$$E_{tot} = E_{dir} + E_{dif}. \tag{9}$$

Thus,

$$r(2\pi; \theta_r, \phi_r) = \frac{1}{E_{tot}}\left[R(\theta_o; \theta_r, \phi_r)E_{dir}(\theta_o) + \int R(\theta_i; \theta_r, \phi_r)L_{dif}(\theta_i, \phi_i)d\omega_i\right] \tag{10}$$

Note our usage of $R(\theta_i;\theta_r,\phi_r)$ for BRF and $r(2\pi;\theta_r,\phi_r)$ for HDRF, $E_{dir}$, $E_{dif}$, and $E_{tot}$ for the direct, diffuse, and total downwelling incident irradiances, and $\theta_o$ for the solar incident angle. The irradiance components are those incident upon a horizontal surface and thus include the $\cos\theta_i$ term of illumination.

The final quantity discussed in this paper is the directional/hemispheric reflectance (DHR). Unlike the previous two quantities, the DHR is not a measure of flux ratioed to an ideal diffuser. Rather, this parameter represents the flux ratio of light reflected into a hemisphere, when the target is illuminated with a narrow cone of light from direction $\theta_o$ to the incident flux. It is written as:

$$\rho(\theta_i; 2\pi) = \frac{d\int L_r(\theta_r, \phi_r)\cos\theta_r d\omega_r}{dE_o(\theta_o)} = \left(d\int R(\theta_i; \theta_r, \phi_r)\cos\theta_r d\omega_r\right)/\pi. \tag{11}$$

For this equation, the reflected radiance was substituted using Eq. (4).

## 2. MISR experiment

As part of the Earth-Observing System (EOS) mission, NASA launched the first of a series of platforms in 1999. The first platform, named Terra, includes instruments to measure geophysical parameters used in the study of the terrestrial surface, atmospheric composition, clouds, aerosols, and radiation balance. The Multi-angle Imaging SpectroRadiometer (MISR) instrument (Diner et al., 1998) is one of five instruments on this platform. Absolute radiometric calibration is to be maintained to within 3% uncertainty throughout the mission. Due to this challenging requirement, an OBC subsystem has been designed as part of the instrument. Elements include a pair of diffuse reflectance standard panels that will be deployed at monthly intervals to reflect solar irradiance into the MISR cameras. Absolute reflectance knowledge of the panels is not required, as MISR makes use of on-board detector standards to establish the radiometric scale. As the cameras and photodiode standards are not co-aligned, relative changes in radiance, reflected in the direction of the cameras as compared to that in the direction of the photodiodes, are required. For this transfer, MISR requires accuracy only in the relative BRF of the panels. That is, we only need know the shape of the BRF curve, and not its absolute scaling factor.

Table 1
MISR radiometric calibration requirements

| Parameter | Requirement at $\rho_{eq} = 1.0$ (%) | Requirement at $\rho_{eq} = 0.05$ (%) |
|---|---|---|
| Absolute | ±3 | ±6 |
| Camera-relative | ±1 | ±2 |
| Band-relative | ±1 | ±2 |
| Pixel-relative | ±0.5 | ±1 |

MISR has been designed and built by the Jet Propulsion Laboratory (JPL). It utilizes nine cameras, which image the Earth in a pushbroom fashion. The cameras are arranged with one nadir camera and two banks of four cameras pointing in the forward and aftward directions with respect to the spacecraft ground track. Images are acquired at the Earth's surface with view angles of 0°, ±26.1°, ±45.6°, ±60.0°, and ±70.5°. Radiometrically calibrated images at each angle will be obtained at the four spectral bands 446, 558, 672, and 866 nm. The nine cameras are designated An, Af/Aa, Bf/Ba, Cf/Ca, and Df/Da. Here, "A" through "D" denote one of four camera designs, ranging from the small (including nadir) to large view angle configurations. Additionally, "f" denotes a forward-pointing camera, "a" an aftward-pointing camera, and "n" the nadir camera.

MISR radiometric calibration requirements are given in Table 1, as specified at the 68% (1σ) confidence level. The absolute calibration goal refers to the transfer of instrument output digital numbers (DNs) into incident radiance values, traceable to Système International (SI) units (Meyer-Arendt, 1968). High accuracy is required for long-term monitoring programs, and to enable change detection. The relative calibration requirements are needed for accurate determination of angular signatures, which in turn enable aerosol retrievals and BRF determination of clouds and surface scenes. In this table, the requirements are defined at two equivalent reflectance levels, $\rho_{eq}$, where the equivalent reflectance is defined to be the measured radiance divided by $E_o/\pi$, and where $E_o$ is the exoatmospheric irradiance weighted by the MISR spectral response function (1867, 1842, 1524, and 977.8 W $m^{-2}$, respectively). In addition to these requirements, those such as stability and signal-to-noise have been defined and are equally critical (Bruegge, Duval et al., 1993).

### 2.1. OBC

The MISR calibration panels are required to be made from a material that has a high, near-Lambertian reflectance. While not in use, the panels are stowed and protected by a labyrinth seal. At approximately bi-monthly time intervals, the panels are deployed for calibration. Fig. 1 shows the nine MISR cameras, with the North Pole panel deployed for calibration. Over the North Pole, this plate will swing aftward to diffusely reflect sunlight into the fields-of-view of the aftward-looking and nadir cameras. Over the South Pole, the other plate will swing forward for calibration of the forward-looking cameras. The nadir camera will view both panels, providing a link between the two sets of observations. The two panels are required to support the fore- and aft-camera views, and South/North observation periods are required to achieve solar illumination of the two panels, respectively. The panels are deployed through an angle of 67.5°, and receive solar illumination at about 45° from nadir. At this geometry, the specular direction will fall mid-way between the B and C cameras, thereby minimizing departures from Lambertian reflectance. (This was a precautionary measure as no specular reflection component has, in practice, been

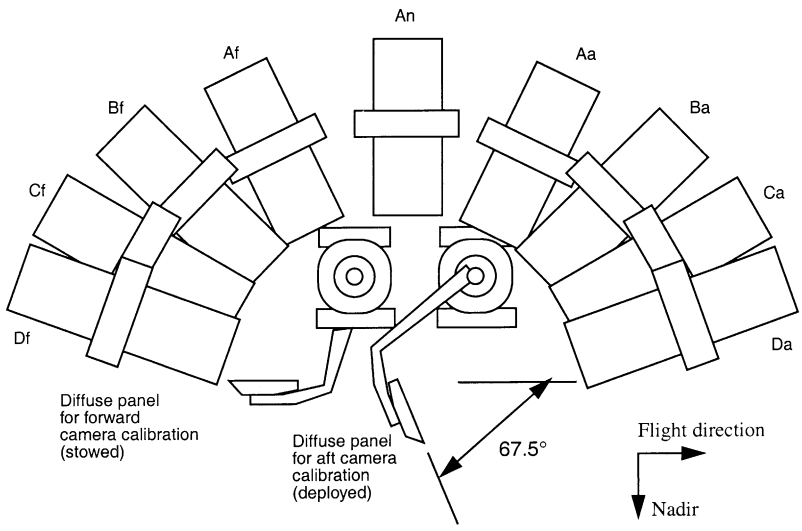


Fig. 1. Diffuse panel deployment for MISR in-flight calibration.

observed.) Cumulative space exposure time (deploy time) for each panel is expected to be no more than 100 h over the 6-year mission life. Flight qualification testing has verified panel reflectance stability (Bruegge, Stiegman, Rainen, & Springsteen, 1993; Stiegman, Bruegge, & Springsteen, 1993).

Six sets of detector standards are used to monitor the radiance reflected from these panels, with each set consisting of four photodiodes filtered to the four MISR spectral passbands. The photodiodes are of two basic designs. Five sets consist of single photodiodes, termed PIN photodiodes. These are mounted at two nadir-viewing positions, at the Da and Df camera viewing positions, and on a goniometer which swings at $\pm 65^\circ$ along the flight direction. An additional photodiode set is constructed in a light trap configuration and uses High Quantum Efficiency (HQE) photodiode technology. The HQE photodiodes are nadir-viewing. As the photodiodes have a field-of-view of 2.5°, and the cameras have a cross-track field of view as large as $\pm 14.9^\circ$ (for the A-designed lens), the photodiodes do not measure light reflected in all of the A and D angle view directions. Nor are there photodiodes in the B or C viewing angle directions. Thus, the panel BRF is used to transfer the diode-measured radiances to those that are incident at the camera view angles. This is provided by the relationship:

$$L^{\mathrm{ccd}}(\theta_{\mathrm{r}}^{\mathrm{ccd}}, \phi_{\mathrm{r}}^{\mathrm{ccd}}) = L^{\mathrm{obc}}(\theta_{\mathrm{r}}^{\mathrm{obc}}, \phi_{\mathrm{r}}^{\mathrm{obc}}) \frac{R(\theta_{\mathrm{o}}; \theta_{\mathrm{r}}^{\mathrm{ccd}}, \phi_{\mathrm{r}}^{\mathrm{ccd}})}{R(\theta_{\mathrm{o}}; \theta_{\mathrm{r}}^{\mathrm{obc}}, \phi_{\mathrm{r}}^{\mathrm{obc}})} \tag{12}$$

Here, $L^{\mathrm{obc}}$ and $L^{\mathrm{ccd}}$ are band-weighted radiances incident onto the OBC photodiodes and CCD pixels, respectively. These radiances are weighted over the four MISR spectral bands.

During on-orbit calibration, data are acquired simultaneously with the photodiode detector standards and the CCD cameras. This occurs throughout a 5-min window, during which the sun transits a range of solar illumination and azimuth angles. These angles are shown in Fig. 2, where here the illumination angles are defined with respect to the panel coordinate system. That is, $\phi_{\mathrm{p}} = 0^\circ$ for illumination along the spacecraft $y$-axis (solar side), and $\theta_{\mathrm{p}} = 0^\circ$ for illumination along the panel normal. (The subscript p indicates the panel coordinate system.) The expected range of view elevations from the MISR cameras is $9-70^\circ$. The anticipated solar incidence angle onto the calibration panels is from 38° to 55°, as measured from the surface normal. The azimuth angles will be on the $\phi_{\mathrm{r}} = 180^\circ$, forward scatter side.

### 2.2. Vicarious calibration (VC)

In addition to assigning a radiometric calibration to the instrument via the OBC, MISR will make use of VC methodologies. Using a desert playa, such as Lunar Lake, the surface HDRF, $r_{\mathrm{surface}}(2\pi;\theta_{\mathrm{r}},\phi_{\mathrm{r}})$, is computed for the MISR view angles. This is done using spectrally filtered radiometers, such as the PARABOLA III (Abdou et al., 1999). The surface HDRF is found from ratioing instrument output voltage, as the instrument views the surface, to that of a Spectralon reflectance standard. The surface HDRF and atmospheric retrievals are used, in conjunction with a radiative transfer code, to compute the top-of-atmosphere radiance incident on MISR. These data provide an on-orbit calibration of the instrument, independent of the OBC calibration. Surface BRF are not required, as our code makes use of the HDRF as an input.

To measure the surface HDRF, first a measure of the radiance that would be reflected from an ideal surface, as required by Eq. (1), is provided by the Spectralon panel corrected for its HDRF. That is (Eq. (13)):

$$L_{\mathrm{ideal}} = L_{\mathrm{spec}}(\theta_{\mathrm{r}}, \phi_{\mathrm{r}}) / r_{\mathrm{spec}}(2\pi; \theta_{\mathrm{r}}, \phi_{\mathrm{r}}). \tag{13}$$

We omit the angular dependence $(\theta_{\mathrm{r}},\phi_{\mathrm{r}})$ when referring to $L_{\mathrm{ideal}}$, as the radiance from an ideal surface is independent of viewing angle. The Spectralon observations are made at a nadir viewing angle, $(\theta_{\mathrm{r}},\phi_{\mathrm{r}})=(0^\circ,0^\circ)$. This ratio is used for all surface HDRF determinations, even at non-nadir viewing angles, as $L_{\mathrm{ideal}}$ is independent of view angle. We thus have:

$$r_{\mathrm{surf}}(2\pi; \theta_{\mathrm{r}}, \phi_{\mathrm{r}}) = L_{\mathrm{surf}}(2\pi; \theta_{\mathrm{r}}, \phi_{\mathrm{r}}) r_{\mathrm{spec}}(2\pi; 0^\circ, 0^\circ) / L_{\mathrm{spec}}(2\pi; 0^\circ, 0^\circ). \tag{14}$$

For field radiometers, where the output voltage is proportional to the incident radiance, we can simplify even further (Eq. (15)):

$$r_{\mathrm{surf}}(2\pi; \theta_{\mathrm{r}}, \phi_{\mathrm{r}}) = V_{\mathrm{surf}}(2\pi; \theta_{\mathrm{r}}, \phi_{\mathrm{r}}) r_{\mathrm{spec}}(2\pi; 0^\circ, 0^\circ) / V_{\mathrm{spec}}(2\pi; 0^\circ, 0^\circ) \tag{15}$$

In this algorithm, knowledge of the Spectralon HDRF is required, specific to the atmosphere and illumination conditions at the time of data acquisition. For clear atmospheric conditions, it can be approximated from the BRF. This is convenient, as the BRF is a property of the panel itself, and not of the panel/atmosphere system. For heavy aerosol optical depths, the BRF approximation is not sufficient. In this case, Eq. (10) would need to be solved, using successive iterations, to retrieve the Spectralon BRF. A measure of the total and diffuse downwelling radiance is required for this solution. We would obtain these data from our PARABOLA III field radiometer.

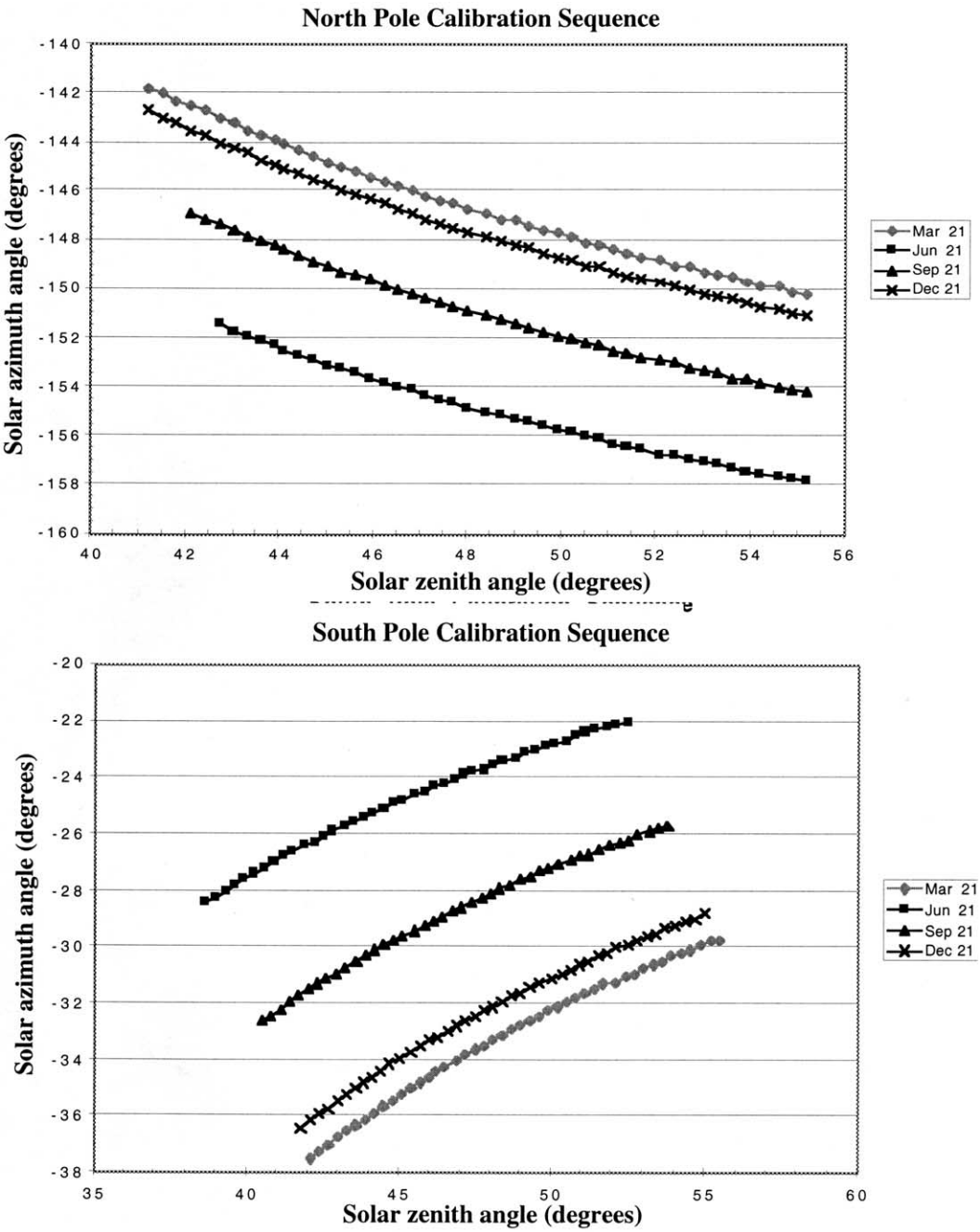


Fig. 2. Solar angles onto the diffuse panel during the North and South pole panel deployments.

### 2.3. Surface BRF retrieval

The MISR validation team makes frequent measurements of surface BRF, for the purpose of validating MISR and AirMISR retrievals. Specifically, we make use of PARABOLA III surface measured upwelling and downwelling radiances, along with the measurement of upwelling radiance for a nadir view of a Spectralon diffuse panel. The Spectralon BRF must be known for the analysis, but these data are accurately determined from laboratory measurements. An accurate surface BRF retrieval is obtained with this approach, independent of radiometer absolute calibration, as the radiances measured over the surface are ratioed with the Spectralon measured upwelling radiances, and any instrument calibration error is cancelled.

Let $R^n$ represent the $n$th estimate of the surface BRF. As an initial guess, we set $R^0 = r(2\pi;\theta_r,\phi_r)$, that is our direct measure of the surface HDRF. For subsequent iterations, we make use of the following expression:

$$R^n_{\text{surf}}(\theta_o;\theta_r,\phi_r) = \frac{L^{\text{meas}}_{\text{dir}}(\theta_r,\phi_r)}{L_{\text{ideal,dir}}} \tag{16}$$

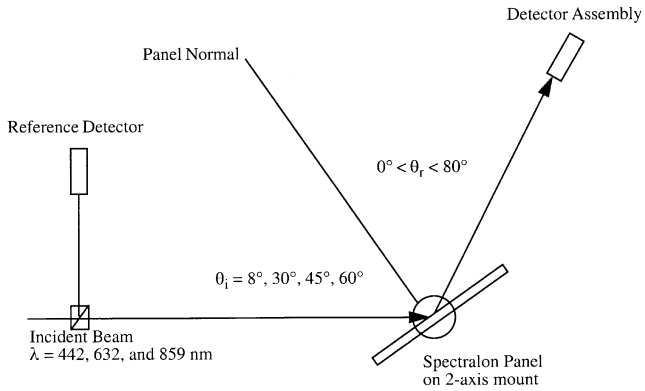


Fig. 3. Optical layout of the BRF test facility.

The numerator is derived from the difference between the total upwelling radiance and the diffuse upwelling radiance. These radiances are due to the reflection from the total surface irradiance and diffuse surface irradiance, respectively (Eq. (17)):

$$L_{\mathrm{dir}}^{\mathrm{meas}}(\theta_r, \phi_r) = L_{\mathrm{total}}^{\mathrm{meas}}(\theta_r, \phi_r) - \pi^{-1} \int R_{\mathrm{surf}}^{n-1}(\theta_i; \theta_r, \phi_r) L_{\mathrm{dif}}^{\mathrm{meas}}(\theta_i) \mathrm{d}\omega_i. \quad (17)$$

The denominator of Eq. (16) is provided in a similar determination (Eq. (18)):

$$L_{\mathrm{ideal,dir}} = (L_{\mathrm{spec,total}}^{\mathrm{meas}}(0°, 0°) - \pi^{-1} \int R_{\mathrm{spec}}(\theta_i; \theta_r, \phi_r) L_{\mathrm{dif}}^{\mathrm{meas}}(\theta_i) \mathrm{d}\omega_i) / (R_{\mathrm{spec}}(\theta_o; 0°, 0°)) \quad (18)$$

As before, a nadir view of the Spectralon is used in the retrieval, and the BRF at this view angle is used to correct

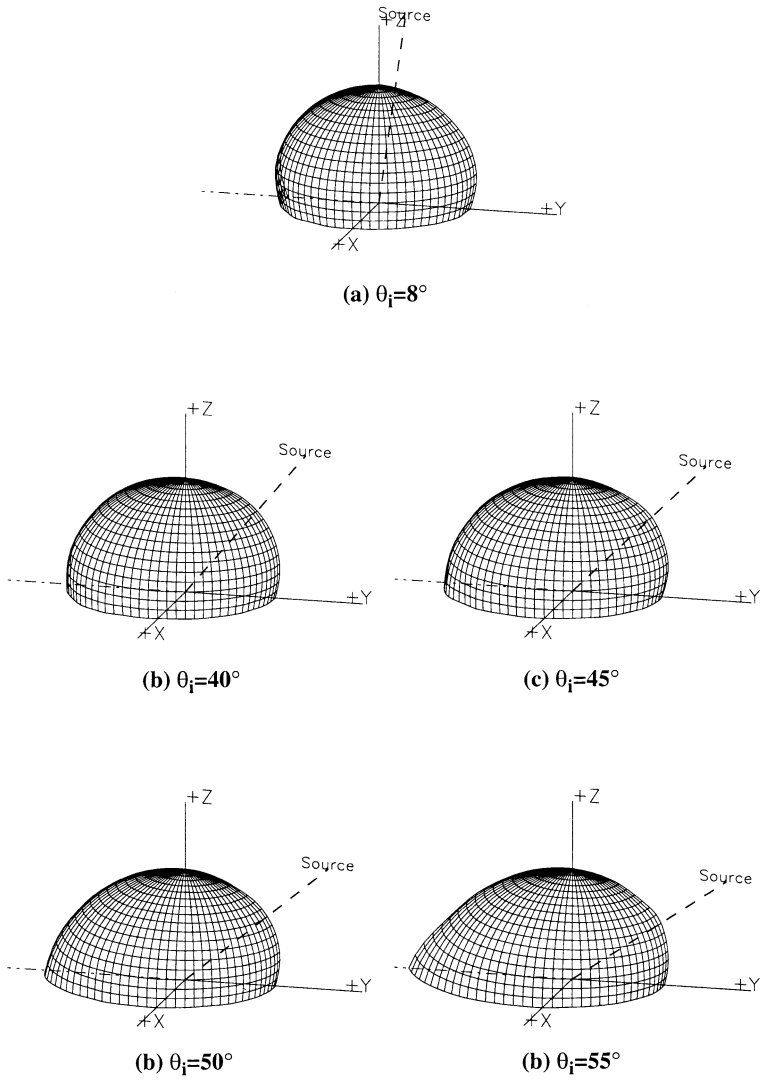


Fig. 4. Measured hemispheric BRF of test piece 12669-2 at 632.8 nm.

for differences from an ideal diffuser. This value is invariant as successive iterations of the surface BRF is determined.

## 3. Spectralon BRF data acquisition

### 3.1. Experimental set-up

Details of the facility used to characterize the Spectralon panels have been described elsewhere (McGuckin, Haner, Menzies, Esproles, & Brothers, 1996), but will be briefly summarized here. A simplified schematic of the set-up is shown in Fig. 3. Laser illumination was chosen for this experiment. This decision was made in order to fulfill the requirement to measure relative BRF to within 0.1% precision. The intensity provided by these laser sources allowed detection to be made with high signal-to-noise. As Spectralon reflectance properties are known to be a slowly varying function of wavelength, the use of broadband illumination or detection was not a priority. Three laser sources were utilized, each within ±5 nm of a MISR spectral band. These sources were a helium cadmium (HeCd) laser at 442 nm, a helium neon laser (HeNe) at 632.8 nm, and a gallium aluminum arsenide (GaAlAs) semiconductor diode laser source at 859.9 nm. Although a convenient source was not found to measure the 558 nm band, the existing sources do allow coverage of the MISR extreme wavelength range.

Commercially available rotation stages control the detector and target rotation. Each is capable of 360° rotation with 0.05° accuracy. A cradle is used to position the target elevation angle, moving ±45° in travel. Care is taken to insure that all rotations are made using an axis that is on the front surface of the panel to be characterized. The set-up was built to completely characterize a target between 2.5 and 10 cm (1 and 4 in.) on a side, or to provide principal plane only viewing angles of the $52.2 \times 7.1 \times 0.71$ cm$^3$ ($20.6 \times 2.8 \times 0.28$ in.$^3$) flight target. The flight target is too large to be rotated out-of-plane, as it would collide with the optical bench table.

The relative amplitude of the light incident upon the Spectralon panel is controlled by a zero-order half-wave plate and polarizer combination. The latter was orientated to pass either s- or p-polarized light relative to the plane containing the detector and the incident beam, termed the principal plane. Scattered light is measured unpolarized, that is without use of a polarization analyzer at the detector. This simplification is permitted in that MISR is a polarization-insensitive instrument; hence, a decoupling of the reflected beam into its polarization states was not needed for this work. (A separate paper, Haner, McGuckin, & Bruegge, 1999, provides the polarization properties of Spectralon reflected light.) A reference detector continually monitors the illumination in order to account for amplitude fluctuations of the source. Both the panel-viewing and reference detectors use 1-cm square silicon photodiodes. Each detection channel uses phase-sensitive detection and amplification, and a 16-bit analog-to-digital (A/D) converter. A personal computer is used for data acquisition and processing.

Table 2
Experimental parameters

| λ (nm) | $\Omega_d$, sr | $10^{ND}$ |
|---|---|---|
| 442 | 8.722e − 4 | 3.126e3 |
| 632 | 8.722e − 4 | 2.838e3 |
| 860 | 8.722e − 4 | 4.074e3 |

Table 3
BRF for a nadir viewing sensor and DHR values at 632.8 nm

| Illumination, $\theta_i$ (°) | BRF, $R(\theta_i;0°)$ | DHR, $\rho(\theta_i;2\pi)$ |
|---|---|---|
| 8 | 1.045 | 0.991 |
| 40 | 1.004 | 0.990 |
| 45 | 0.994 | 0.993 |
| 50 | 0.983 | 0.983 |
| 55 | 0.972 | 0.990 |

Data were acquired at 632.8 nm and varying illumination angles.

### 3.2. Experiment plan

The full-hemisphere BRF measurements were performed on test pieces, as the laboratory set-up did not allow such measurements to be done on the actual flight units (Fig. 4). These test pieces were manufactured simultaneously with the flight panels, as each was cut from the same tile. Packing density, baking, and sanding histories were identical, and thus test piece BRF data were acquired to serve as proxy for flight hardware reflectance values.

Based upon the viewing geometries depicted by Fig. 2, the measurement plan elected was to provide data acquisition at illumination angles of 40°, 45°, 50°, and 55°. In addition, an illumination of 8° was provided in order to make a verification of the BRF scale, by comparison with the DHR provided with the targets by the vendor. (Recall DHR was defined by Eq. (11)). The sampling strategy for the reflected light was such that an integration of the directional values would allow DHR computation. For each angle of incidence, the detector viewed the reflected signal at elevation angles of 1°, 10°, 20°, 30°, 40°, 50°, 60°, 70°, and 80° and azimuth angles from 0° to 180° at a sampling interval of 10°. Symmetry in the BRF distribution for azimuth angles from 180° to 360° was assumed.

### 3.3. Data reduction

The MISR reflectance data consist of two measurements: the incident signal, $V_i$,, and the reflected signal, $V_r$ (Eq. (19)):

$$R(\theta_i;\theta_r,\phi_r) = \left[\frac{V_r(\theta_r,\phi_r)}{V_{r,ref}(\theta_r,\phi_r)}\right] \Big/ \left\{\left[\frac{V_i(\theta_i)}{V_{i,ref}(\theta_i)}\right]\Omega_d 10^{ND}\cos\theta_r\right\}, \qquad (19)$$

Table 4
BRF at MISR view angles, 45° incident angle, and 632.8 nm illumination

| | | BRF, $R(45°;\theta_r,\phi_r)$ vs. view azimuth, $\phi_r$ | | | | |
|---|---|---|---|---|---|---|
| Camera name | View angle, $\theta_r$ (°) | 0° | 45° | 90° | 135° | 180° |
| An | 0 | 0.995 | 0.995 | 0.995 | 0.995 | 0.995 |
| Af/Aa | 26.1 | 0.982 | 0.985 | 0.995 | 1.010 | 1.020 |
| Bf/Ba | 45.6 | 0.970 | 0.967 | 0.988 | 1.021 | 1.047 |
| Cf/Ca | 60.0 | 0.926 | 0.945 | 0.979 | 1.027 | 1.069 |
| Df/Da | 70.5 | 0.886 | 0.918 | 0.968 | 1.030 | 1.093 |

where $\Omega_d$,sr is the detector solid angle, $10^{ND}$ refers to the neutral density filter used in calibration, and $V_{i,ref}$ and $V_{r,ref}$ are values of the incident and reflective beams, respectively, as acquired by the reference detector. Table 2 gives the spectral constants for this experiment, including the measured spectral transmittance of the neutral density filters at our wavelengths.

Measurements are taken for both s-polarization incident and p-polarization incident illumination conditions. These data are then converted to BRF, that for an unpolarized source, by taking the average of the s-polarization incident and p-polarization incident BRFs (Eq. (20)):

$$R_{unpol}(\theta_i;\theta_r,\phi_r) = [R_s(\theta_i;\theta_r,\phi_r) + R_p(\theta_i;\theta_r,\phi_r)]/2. \quad (20)$$

The measured BRF was resampled via spline interpolation/extrapolation and a numerical integration over the hemisphere was performed to arrive at the DHR (see Table 3). Specifically, a second-order polynomial fit to the data was done in the $\theta_i$ dimension, and a spline fit was done in each of the $\theta_r$ and $\phi_r$ dimensions. The DHR (interpolated to 632 nm) measured by Labsphere for a source at 8° for the same sample was 0.983, a 0.8% difference from our result. Some discrete values of the BRF are given in Tables 3 and 4. A summary of the complete BRF results is given in Fig. 4.

For processing of on-orbit data, MISR has resampled the measured BRF data to 2° intervals throughout the hemisphere. A linear interpolation is then used to find illumination and view-angle-specific values.

## 4. Sensitivity studies

### 4.1. Wavelength

Comparisons of the principal plane BRF data at 632.8 nm with that acquired at 442 and 860 nm are shown in Fig. 5. Peak-to-peak differences are found to be as large as 2.5%, with a standard deviation of 1%. In order to validate absolute BRF measurements, a multicenter comparison of BRF measurements of Spectralon was conducted. These validation data have been published in Early et al. (1999). Results validate the JPL measure of BRF to within 2%, 0.5%, and 0.5%, respectively, at three wavelengths 442, 632, and 860 nm. This comparison is made with comparable measurements made by the National Institute of Standards and Technology (NIST). The NIST data show Spectralon BRF to be spectrally flat throughout the visible spectrum, for small incident and view angles (e.g., 45°, 0°, respectively). For larger incident and view angles, e.g., (60°; 60°), changes in BRF can be several percent with wavelength.

Of greater interest to the MISR project, however, is a validation of our relative BRF data. Early et al. (1999) show agreement between NIST and JPL, to better than ±0.5% at all three wavelengths, for relative BRF data measures. As shown in Eq. (12), it is only the accuracy of these relative BRF data that impacts the calibration of the MISR instrument.

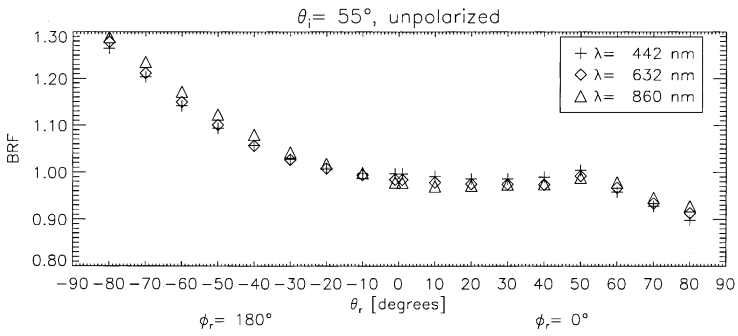


Fig. 5. Principal plane BRF with wavelength.

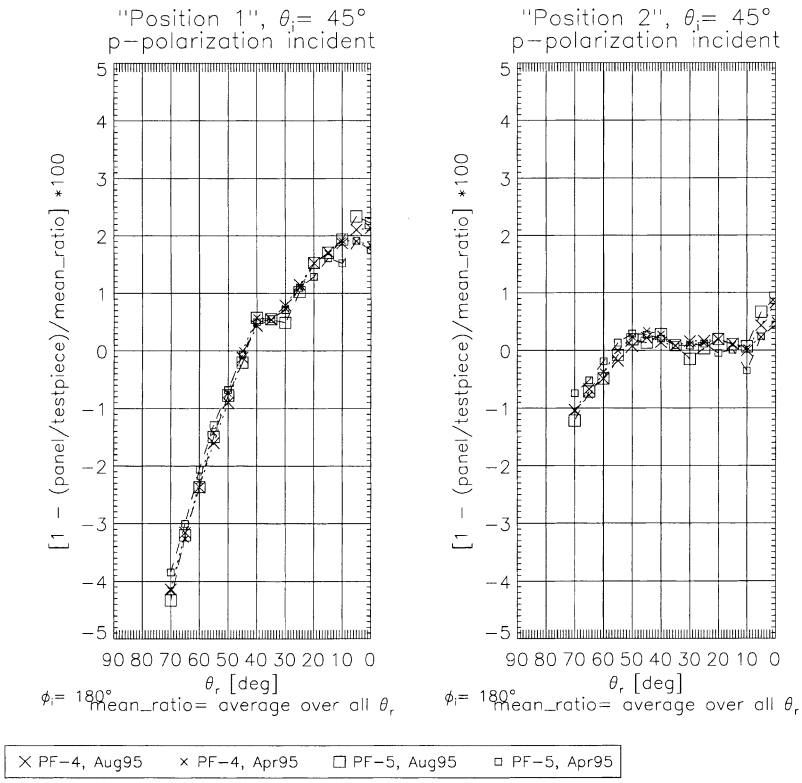


Fig. 6. Relative difference between flight panels and test piece. Test piece Position 1 was not representative, due to an imperfection at this location.

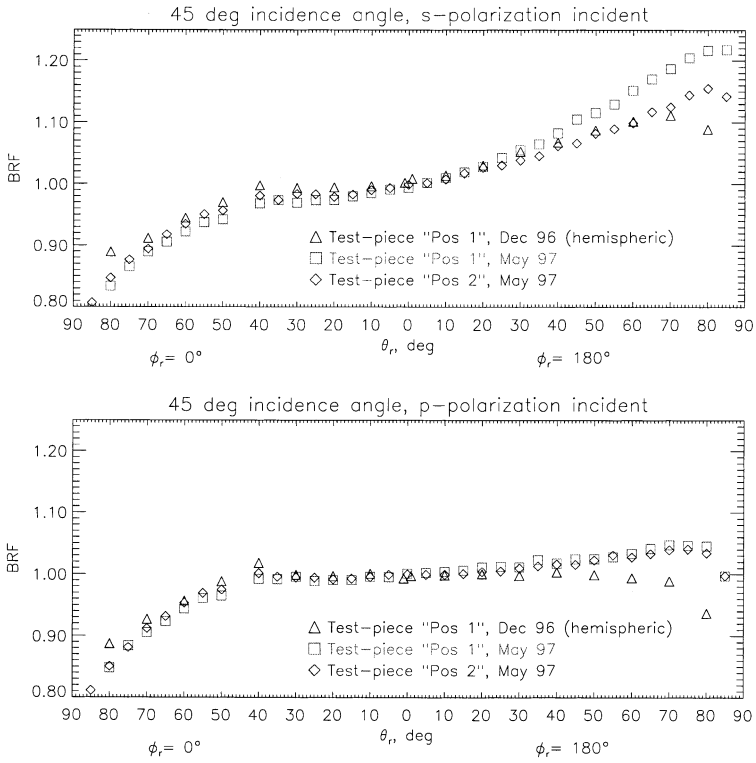


Fig. 7. BRF components for s- and p-incident light.

Table 5
BRF error sources

| Error source | Error in relative BRF (%) | Error in absolute BRF (%) |
|---|---|---|
| Panel uniformity | 1 | 1 |
| Wavelength variability | 1 | 2.5 |
| Panel thickness | 0.05 | 0.05 |
| Laser speckle | 0.05 | 0.05 |
| Angular accuracy | 0.15 | 0.15 |
| Detector SNR | 0.05 | 0.05 |
| Detector linearity | 0.05 | 0.05 |
| $\Omega_d 10^{ND}$ product | Not applicable | 1 |
| Root sum square total | 1.4 | 2.9 |

### 4.2. Target/target differences

Fig. 6 shows a comparison of the BRF in the principal plane for both the test piece and flight panels. During this study, it was discovered that the test piece had two distinct regions to it. Rotation of the test piece by 90° in the laboratory measurement set-up did not affect the result. The flight panels, which are much longer than the test piece, exhibited greater spatial uniformity in the BRF. It was subsequently noted that there was a slight dip in the test piece in the vicinity of Position 1, which was previously undetected by visual inspection. As shown in the figure, data acquired at test piece Position 2 better matched the BRF results obtained from the flight units. The data from this position are the ones delivered for MISR in-flight calibrations and are referred to as "the Spectralon BRF data base." The discovery of the depression is a reminder to us that any arbitrary panel may differ in local BRF due to surface flaws, such as scratches and digs.

Fig. 7 shows the differences in the reflectance of Spectralon for s- and p-illumination conditions. As mentioned above, Position 2 data are used as representative of the flight panel. It is the average of these data that are used to construct the BRF appropriate for unpolarized illumination. It is the unpolarized BRF that is applicable to our calibration applications. A further study on differences in reflectance properties with polarization is provided by Haner et al. (1999).

## 5. BRF uncertainty estimation

### 5.1. Experimental errors

An error analysis of the BRF values is provided in Table 5. The values for the two largest error sources, that of the panel uniformity and wavelength variability, are motivated from studies such as that described above. Other sources of error are not precisely known, but are thought to be negligible (McGuckin, Haner, & Menzies, 1997) and are written here with an over estimation of 0.05. We see that our uncertainty in relative BRF is large (1.4%), but sufficient to achieve a 3% absolute calibration. The camera-relative and band-relative calibration requirements will only be met if panel uniformity and wavelength variability are, in practice, less than the conservative estimates given here. It is for these reasons that the MISR OBC may best be viewed as determining the absolute radiance scale for the cameras, and that multiple calibration methodologies remain important to the MISR program. Camera-relative calibrations will accurately be made using AirMISR (a single-camera instrument gimbaled to the MISR angles) and histogram equalization techniques (using a statistical compilation of Earth observations). This method will supplement the OBC relative calibration.

### 5.2. Data validations

In addition to the error analysis described above, several validation exercises were carried out. These studies are summarized in the matrix provided in Table 6.

These studies were the following.

• EOS-RR: A comparison of BRF as acquired during an EOS round-robin experiment (Barnes et al., 1998; Early et al.,

Table 6
Spectralon BRF validation study matrix

| Study name | Parameter, illumination angle, $\theta_i$, and wavelengths compared | Sample measured by JPL | Comparison sample | Results |
|---|---|---|---|---|
| EOS-RR | principal plane BRF at 30°, 45°, and 60° | NIST provided | Same target | Agreement within 0.5%, relative BRF; 0.5% absolute at 632 nm |
| RIT | principal plane BRF at 45° (hemispheric data available) | Test piece[a] | Unrelated sample | Agreement to within 5% for view angles to 30°, 15% differences in the forward scattered direction for larger angles |
| TMA | principal plane BRF at 45° and 632 nm | Test piece[a] | Unrelated sample | Agreement is within 1% for view angles to 60° and 5% to 70° |
| Model | hemispheric BRF at 632 nm | Test piece[a] | Unrelated sample | 1–5% |
| Labsphere | DHR at 8°, 632 nm | Test piece[a] | Same target | Agreement within 0.8% |

[a] This is the same test piece as was used to develop the MISR BRF database, serial no. 12669-2.

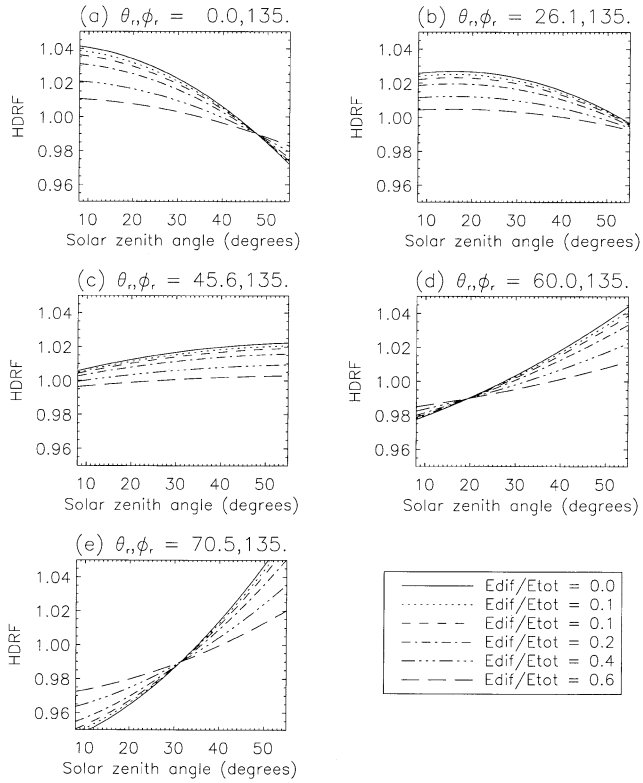


Fig. 8. Variations in HDRF for various $E_{dir}/E_{tot}$ irradiance conditions. Plots (a) through (e) give results for MISR cameras An through D, respectively.

1999). Agreement with the NIST was excellent, verifying our data methodology and data reduction procedures.

- RIT: A comparison of our full-hemisphere Spectralon BRF data base to that reported by the Rochester Institute of Technology (Feng et al., 1993) was made. Differences were larger than other comparisons; however, sample differences are possible.
- TMA: A comparison of our principal plane Spectralon BRF data base to that reported by TMA technologies showed excellent agreement though different samples were measured.
- Model: A comparison of our full-hemisphere Spectralon BRF data base to a Spectralon model reported in the literature (Flasse, Verstraete, Pinty, & Bruegge, 1993). The model was generated using the principal plane TMA data. Differences might have been smaller had the model been developed using the test piece hemispheric BRF data.
- Labsphere: A comparison of our integrated DHR values to those reported by Labsphere showed good agreement.

The most definitive verification of our data accuracy comes from the EOS round-robin experiment. Here, common samples were measured at the respective facilities. With agreement to within 2% and 0.5% for the absolute and relative BRF measurement, this study supports our BRF uncertainty estimates provided in Table 5. (Further, it supports agreement at 632 nm to within 0.5% absolute.) Our error uncertainty is larger than the RR agreement numbers. This is to allow for the uncertainty in wavelength and panel spatial uniformity.

## 6. Spectralon BRF/HDRF differences

For VC applications, the Spectralon panel HDRF must be known for the specific diffuse plus solar/direct irradiance conditions present at the moment the panel is measured, as shown by Eq. (14). As this HDRF varies temporally with changing solar angle and with atmospheric conditions, it cannot be determined a priori. For clear atmospheric conditions, particularly at the longer wavelengths, it may be approximated by the BRF. The BRF, conversely, is an inherent property of Spectralon, and can simply be read from a data base, such as that presented in this paper.

The differences between BRF and HDRF have been detailed in the literature. An excellent discussion is given, e.g., in Gu and Guyot (1993). These authors make the observations that:

- wavelength and atmospheric visibility effect HDRF through changes in the diffuse to direct surface irradiance;
- for an isotropic distribution of the surface irradiance, the HDRF (directional in view angle) is numerically equivalent to the DHR (directional in illumination angle) due to Helmholtz reciprocity principle;
- for direct only illumination, the HDRF is equivalent to the BRF;
- the HDRF for any arbitrary field condition lies between the BRF and the DHR of the surface; and
- differences in BRF and DHR are minimal for a reflectance standard that approaches Lambertian behavior.

These general observations are applicable to the retrievals of surface reflectances at off-nadir views, as of interest in our MISR validation studies. As Spectralon diffusers do indeed approach Lambertian behavior, particularly for small solar incident angles, we expect the HDRF to be reasonably represented by the BRF. This assumption would not normally be made for arbitrary surfaces, i.e., diffusers not as Lambertian as Spectralon. Expanding upon the work of Gu and Guyot (1993), we estimate the error here for a range of

Table 7
Diffuse to total irradiance ratios vs. visibility at 550 nm

| | $E_{dir}/E_{tot}$ vs. visibility (km) | | |
|---|---|---|---|
| $\theta_o$ (°) | 10 | 50 | 999 |
| 25.1 | 0.39 | 0.19 | 0.053 |
| 47.3 | 0.46 | 0.23 | 0.72 |
| 65.9 | 0.63 | 0.34 | 0.12 |

sensor viewing angles. Their approach assumes, for any real atmosphere, that the differences in these two functions falls somewhere between the direct beam ($E_{dif}=0$) case and the isotropic diffuse irradiance condition with a known $E_{dif}/E_{tot}$ ratio. Making use of Eq. (10) with the isotropic assumption, we have:

$$\begin{aligned} r(2\pi;\theta_r,\phi_r) &= R(\theta_i;\theta_r,\phi_r)E_{dir}/E_{tot} + \rho(\theta_r;2\pi)E_{dif}/E_{tot} \\ &= R(\theta_i;\theta_r,\phi_r)(1 - E_{dif}/E_{tot}) \\ &\quad + \rho(\theta_r;2\pi)(E_{dif}/E_{tot}) \end{aligned} \tag{21}$$

The results of such a study are presented in Fig. 8 for a range of solar elevation angles and the MISR camera view angles. For simplicity, a single azimuthal view angle of 135° is selected. In order to compare these $E_{dif}/E_{tot}$ ratio cases to specific atmospheric conditions, the data values published in Gu and Guyot, and shown in Table 7, are referenced. We note that in the limiting case of direct beam illumination, the HDRF is identically equal to the BRF. For an extreme case of diffuse only illumination ($E_{dir}=0$), the HDRF would be equal to the DHR. A more realistic worst-case diffuse illumination is that depicted in the figure, $E_{dif}/E_{tot}=0.6$. For this computation, a DHR of 0.99 was assumed, consistent with the findings reported in Table 3. By inspection of Eq. (21), it is seen that the ratio $E_{dir}/E_{tot}$ can be solved for directly, given an acceptable tolerance in HDRF vs. BRF. This is given as (Eq. (22)):

$$E_{dif}/E_{tot}(\theta_i;\theta_r,\phi_r) = \frac{R(\theta_i;\theta_r,\phi_r) \times \text{tolerance}}{R(\theta_i;\theta_r,\phi_r) - \rho(\theta_i;2\pi)} \tag{22}$$

Results of this study are presented in Fig. 9. By comparing these results to that of Table 7, we see that the BRF approximation is valid, provided the atmosphere is reasonably clear. These conclusions could not have been made had the Spectralon not been sufficiently Lambertian.

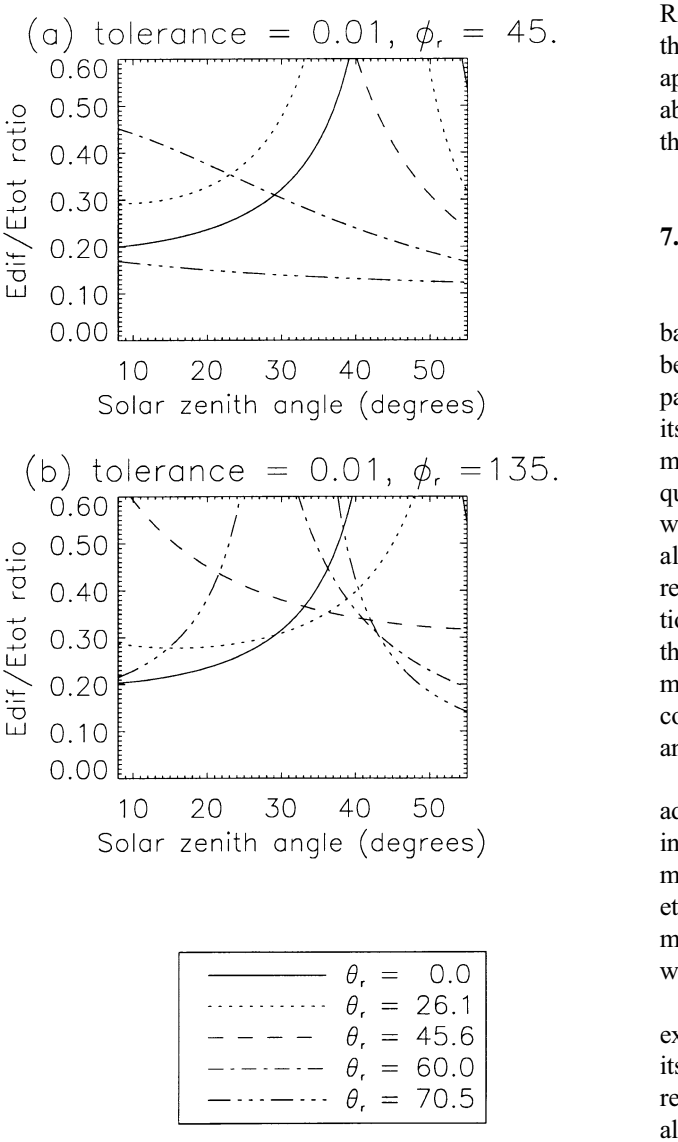


Fig. 9. Upper bound on $E_{dir}/E_{tot}$ required to achieve HDRF and BRF agreement within a tolerance of 0.01. (a) and (b) give examples for two view azimuths.

## 7. Conclusions

The MISR team has developed a Spectralon BRF data base for use in its on-board and VC experiments. Care has been taken to investigate the generality of the BRF from panel to panel or positions within a panel, and to understand its dependence on wavelength. We believe that the BRF measured here at 632 nm is representative of any high-quality panel to within 1% (to view angles out to 50°) or to within 2% for view angles out to 70°. This uncertainty will allow us to meet our absolute radiometric calibration requirement of 3%. The camera- and band-relative calibrations will be more challenging with this approach. It is for this reason that MISR also makes use of other calibration methodologies, such as the response determined from compiling Earth scene statistics (histogram equalization) and AirMISR underflights.

The potential for on-orbit degradation of the BRF is not addressed here. A previous study (Bruegge et al., 1991) has indicated that the BRF is invariant upon panel yellowing. To monitor this assumption, MISR has incorporated a goniometer within the OBC. Should a change in the BRF profile be measured, the uncertainty in the radiometric calibration would increase.

For the clear atmospheric conditions desired for VC experiments, the HDRF of Spectralon is found by using its BRF approximation. PARABOLA III data allow the retrieval of Spectralon HDRF, where conditions do not allow the BRF approximation to be made. More importantly, PARABOLA III data, in conjunction with knowledge of the Spectralon BRF, are used to determine the BRF of surface targets.

## Acknowledgments

Art Springsteen of Labsphere is to be thanked for providing many of the references and comparison data sets quoted here, and for his many helpful discussions. Yvonne Barnes and Ted Early of the National Institute of Standards and Technology are to be thanked for conducting the EOS round-robin BRF comparison experiment. The TMA data used in the validation study were supplied by Jim Irons, Goddard Space Flight Center. David Haner is also affiliated with the California State Polytechnic University, Pomona, CACA. The work described in this paper is being carried out by the Jet Propulsion Laboratory, California Institute of Technology, under contract with the National Aeronautics and Space Administration.

## References

Abdou, W. A., Bruegge, C. J., Helmlinger, M. C., Gaitley, B. J., Ledeboer, W. C., Pilorz, S. H., Conel, J. E., & Martonchik, J. V. (1999). Vicarious reflectance-based absolute radiometric calibration of AirMISR. *Remote Sensing of the Environment (*this issue).

Barnes, P. Y., Early, E. A., Johnson, B. C., Butler, J. J., Bruegge, C. J., Biggar, S., Spyak, P. R., & Pavlov, M. (1998). Intercomparisons of reflectance measurements. In: Proc. SPIE 3425, Optical diagnostic methods for inorganic transmissive materials, San Diego, July 20–21.

Bruegge, C. J., Duval, V. G., Chrien, N. L., & Diner, D. J. (1993). Calibration plans for the multi-angle imaging spectroradiometer (MISR). *Metrologia*, *30* (4), 213–221.

Bruegge, C. J., Stiegman, A. E., Coulter, D. R., Hale, R. R., Diner, D. J., & Springsteen, A. W. (1991). Reflectance stability analysis of Spectralon diffuse calibration panels. In: *Calibration of passive remote observing optical and microwave instrumentation SPIE*, 1493. Orlando, FL, April 3–5, pp. 132–142.

Bruegge, C. J., Stiegman, A. E., Rainen, R. A., & Springsteen, A. W. (1993). Use of Spectralon as a diffuse reflectance standard for in-flight calibration of Earth-orbiting sensors. *Optical Engineering*, *32* (4), 805–814.

Diner, D. J., Beckert, J. C., Reilly, T. H., Bruegge, C. J., Conel, J. E., Kahn, R., Martonchik, J. V., Ackerman, T. P., Davies, R., Gerstl, S. A. W., Gordon, H. R., Muller, J.-P., Myneni, R., Sellers, R. J., Pinty, B., & Verstraete, M. M. (1998). Multiangle Imaging SpectroRadiometer (MISR) description and experiment overview. *IEEE Transactions on Geoscience Remote Sensing*, *36*, 1072–1087.

Early, E. A., Barnes, P. Y., Johnson, B. C., Butler, J. J., Bruegge, C. J., Biggar, S., Spyak, P. R., & Pavlov M. M. (2000). Bidirectional reflectance round-robin in support of the Earth-Observing System program. *American Meteorological Society*, pp. 1077–1091 (August).

Feng, X., Schott, J. R., & Gallagher, T. (1993). Comparison of methods for generation of absolute reflectance factor values for bidirectional reflectance distribution function studies. *Applied Optics*, *32* (7), 1234–1242.

Flasse, S. P., Verstraete, M. M., Pinty, B., & Bruegge, C. J. (1993). Modeling Spectralon's bidirectional reflectance for in-flight calibration of Earth-orbiting sensors. In: *Recent advances in sensors, radiometric calibration, and processing of remotely sensed data Proceedings of SPIE*, 1938. pp. 100–108 (April).

Gu, X.-F., & Guyot, G. (1993). Effect of diffuse irradiance on the reflectance factor of reference panels under field conditions. *Remote Sensing of the Environment*, *45*, 249–260.

Haner, D., McGuckin, B. T., & Bruegge, C. J. (1999). Polarization characteristics of Spectralon illuminated by coherent light. *Applied Optics*, *38* (30), 6350–6356.

Jackson, R. D., Clarke, T. R., & Moran, M. S. (1992). Bidirectional calibration results for 11 Spectralon and 16 $BaSO_4$ reference panels. *Remote Sensing of the Environment*, *40*, 231–239.

Labsphere. (1998). *Reflections Newsletter*, pp. 1–4 (September).

McGuckin, B. T., Haner, D. A., & Menzies, R. T. (1997). Multiangle Imaging SpectroRadiometer: optical characterization of the calibration panels. *Applied Optics*, *36* (27), 7016–7022.

McGuckin, B. T., Haner, D. A., Menzies, R. T., Esproles, C., & Brothers, A.M. (1996). Directional reflectance characterization facility and measurement methodology. *Applied Optics*, *35* (24), 4827–4834.

Meyer-Arendt, J. R. (1968). Radiometry and photometry: units and conversion factors. *Applied Optics*, *7*, 2081–2084.

Nicodemus, F. E., Richmond, J. C., Ginsberg, I. W., Hsia, J. J., & Limperis, T. (1977). Geometrical considerations and nomenclature for reflection. National Bur. Stand. U.S. Monograph 160.

Stiegman, A. E., Bruegge, C. J., & Springsteen, A. W. (1993). Ultraviolet stability and contamination analysis of Spectralon diffuse reflectance material. *Optical Engineering*, *32* (4), 799–804.

Weidner, V. R., & Hsia, J. J. (1981). Reflectance properties of pressed polytetrafluoroethylene powder. *Journal of the Optical Society of America*, *71*, 856–861.